Supplementary Information for

Large-inductance superconducting microstrip photon detector enabling 10 photon-number resolution

Authors

Ling-Dong Kong[1,3†*], Tian-Zhu Zhang[1,3†], Xiao-Yu Liu[1,3], Hao Li[1,3], Zhen Wang[1,3], Xiao-Ming Xie[1,3] and Li-Xing You[1,2,3*]

Affiliations

[1]National Key Laboratory of Materials for Integrated Circuits, Shanghai Institute of Microsystem and Information Technology, Chinese Academy of Sciences (CAS), Shanghai 200050, China

[2]Center of Materials Science and Optoelectronics Engineering, University of Chinese Academy of Sciences, Beijing 100049, China

[3]CAS Center for Excellence in Superconducting Electronics, Shanghai 200050, China

[†]These authors contributed equally: Ling-Dong Kong, Tian-Zhu Zhang

*Correspondence authors. Email: ldkong@mail.sim.ac.cn (L.-D.K.); lxyou@mail.sim.ac.cn (L.-X.Y.)

1 Discussions on detection performance

We assessed other basic detection performances of the SMSPD at the operation temperature of 2.2 K. Figure S1a shows the normalized photon count rate (PCR) versus bias current at wavelengths of 532 nm, 850 nm, 1064 nm, and 1550 nm. Weak saturation of PCR is observed at the wavelength of 532 nm, which indicates a near-unity intrinsic quantum efficiency. At longer wavelengths, the PCR gradually deviates from saturation and the quantum efficiency reduces. It is recommended to focus on optimizing the superconducting films to address this issue. Additionally, the micrometer-scale strip width and high fill factor of the SMSPD make it little sensitivity to polarization. At the wavelength of 1550 nm, the maximum and minimum PCR for different polarization at a constant photon flux only differ by a ratio of less than 1.02, which aligns with previous findings[37,38]. At the bias current of 116 μA (95% I_{sw}), the system detection is 5.7% at the wavelength of 1064 nm and 5.6% at 1550 nm. The dark count rate (DCR) and timing jitter exhibit similarities to other SMSPDs. The DCR shows an exponential dependence on bias current (Fig. S1b) and reaches 13 c.p.s. at 116 μA (95% I_{sw}) where we performed the PNR measurement. We used a 1550 nm sub-ps pulsed laser to determine the difference between the arrival time of response pulses and Sync time when the detector was biased at 116 uA. The timing jitter defined as the FWHM of the histogram was 108 ps (Fig. S1c). Due to the large kinetic inductance of the detector, the reset time constant (L/R=120 ns) is longer than that of a traditional SNSPD but far smaller than other PNRDs such as TES.

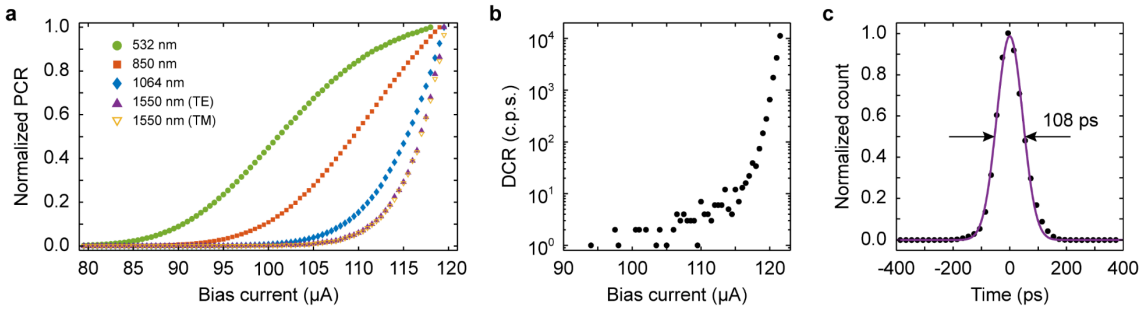

Fig. S1 | Detection performance of the SMSPD. a, Normalized photon count rate as a function of the bias current at wavelengths from visible to infrared. **b**, Dark count rate versus bias current. **c**, Histogram

of the difference between the photon-arrival time and a reference time at 1550 nm in the single-photon regime. The FWHM timing jitter is 108 ps.

The SMPNRD is characterized by high fidelity and a large dynamic range in terms of photon number readout. However, in order to achieve high PNR fidelity, the top priority should be in increasing the device detection efficiency. The first step is to enhance the internal quantum efficiency. Several methods have been experimentally demonstrated to achieve saturated quantum efficiency, such as tuning the film components for high normal-state resistivity[54], ion irradiation[37], and utilizing low-energy-gap films[36,38]. The preferred options should be high-resistivity film and ion irradiation methods, because the high critical temperature T_c and high critical current density j_c they maintain enable a high SNR of readout pulses at an appropriate operating temperature, which is critical for efficient photon number readout as illustrated in Fig. 2. For instance, the 1-μm-wide NbN superconducting microstrips by ion irradiation[37] and 0.89-μm-wide NbN superconducting microstrips with high-resistivity[54] in previous reports individually achieved high switching current of 97 μA and 80 μA at 0.8 K, which are close to the switching current of 122 μA in our SMSPD. Now it appears that using low-energy-gap films like WSi or MoSi may not be ideal candidates, since their switching currents are generally several times lower than that of high-T_c films under equivalent conditions[36,38]. The optical absorption of the detector can be optimized by integrating an optical cavity. Numerical simulation in Fig. S2 shows that our detector can achieve over 97% absorptance at the wavelength of 1550 nm when the microstrips are stacked on top of the distributed Bragg reflector (DBR), which consists of 13 period (26 layer) SiO_2/Ta_2O_5 dielectric layers of optical thickness λ/4[37].

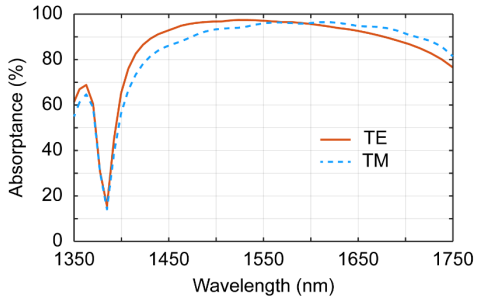

Fig. S2 | Simulated optical absorbance spectra at two orthogonal polarizations of light.

2 Electrothermal simulation based on the two-temperature model

To accurately quantify the dependence of rising-edge time on these variables, we conducted a 2D finite-element electrothermal simulation based on the two-temperature model[55] and modified nonlinear temperature relationship[56,57]. The energy balance equation for the electron subsystem is described by:

$$C_{\mathrm{e}}\frac{\partial(T_{\mathrm{e}})}{\partial(t)} = \nabla^2(\kappa_{\mathrm{e}}T_{\mathrm{e}}) - \frac{C_{\mathrm{e}}}{5T_{\mathrm{e}}^4\tau_{\mathrm{e\text{-}ph}}}\left(T_{\mathrm{e}}^5 - T_{\mathrm{ph}}^5\right) + j^2\rho(T_{\mathrm{e}}), \tag{S1}$$

while the photon subsystem is given by:

$$C_{\mathrm{ph}}\frac{\partial\left(T_{\mathrm{ph}}\right)}{\partial(t)} = \nabla^2\left(\kappa_{\mathrm{ph}}T_{\mathrm{ph}}\right) + \frac{C_{\mathrm{ph}}}{5T_{\mathrm{e}}^4\tau_{\mathrm{ph\text{-}e}}}\left(T_{\mathrm{e}}^5 - T_{\mathrm{ph}}^5\right) - \frac{C_{\mathrm{ph}}}{4T_{\mathrm{ph}}^3\tau_{\mathrm{esc}}}\left(T_{\mathrm{ph}}^4 - T_{\mathrm{sub}}^4\right). \tag{S2}$$

The electrical equation couples the total hotspot resistance $R_{hs}(n)$ which is the integration of resistivity over the nanostrip, the kinetic inductor L_k, the capacitor C_{bt} of the bias-T, and the 50 Ω load Z_0. We set each initial hotspot as a 20-nm-width section across the nanostrip with critical temperature to simulate a single-photon detection or a dark count event. Here, we only focus on changing the kinetic inductance L_{k} and nanostrip's width w at a fixed sheet resistance R_{sq} at different hotspot numbers n, because they are both easy to be tuned during the fabrication process.

Figure S3b presents the simulated four typical 2D profiles of sheet resistance when the total resistance reaches its maximum at different hotspot events. The nanostrip's width is 100 nm and the kinetic inductance is 1 μH. Notably, *n* initial hotspots induce *n* resistive regions, but the resistance increases sublinearly with the hotspot number *n*, which is consistent with the theoretical derivation in Eq. (4) and recent simulated results using a SPICE model[35]. Upon examining the dynamic process of the electrothermal feedback, it becomes clear that a greater number of hotspots generate larger resistance, which in turn pushes the current to leave the nanostrip more quickly and prevents the resistive region from expanding larger. At the corner, the hotspot can only grow towards the direction of the straight section, resulting in a smaller growth compared to that in the straight section and a consequently smaller hotspot resistance in this region. By exploiting this mesoscopic phenomenon, we can potentially reduce

the intrinsic dark counts produced at bends if coupling all the incident photons onto the straight nanostrips.

Figure S3c-e illustrate the influence of kinetic inductance L_{k} on photon-number discrimination. The nanostrip's width is fixed at 100 nm. Figure S3c shows the dynamic changes of hotspot resistance at different photon numbers and kinetic inductances. The maximum resistance increases with the total kinetic inductance but in a sublinear manner, causing the rising edge of generated electrical voltage to be stretched. By numerically fitting these rising-edge times with Power functions (Fig. S3e), we find that they scale with the photon number and total kinetic inductance:

$$\tau_{\mathrm{rise}}(n, L_{\mathrm{k}}) \propto \frac{L_{\mathrm{k}}^{0.44}}{n^{0.5}}. \tag{S3}$$

This formula generally is consistent with the reported results $\tau_{\mathrm{rise}} \propto \sqrt{l/n}$[34], where l is the nanostrip's length proportional to kinetic inductance.

Figure S3f-h illustrate the effect of nanostrip width w on photon-number discrimination, where the kinetic inductance is set at 1 μH. The nanostrip's width directly affects the resistance of unit length. From Fig. S3f, a wider superconducting nanostrip induces a smaller hotspot resistance, which consequently leads to the rising-edge stretching of generated voltage signals (Fig. S3g). The rising-edge time also has a Power function relationship with the nanostrip's width:

$$\tau_{\mathrm{rise}}(n, w) \propto \frac{w^{0.36}}{n^{0.5}}. \tag{S4}$$

Therefore, like a kinetic inductance does in Eq. (S3), a wider nanostrip will make the difference of rising-edge time of adjacent photon number more distinguishable.

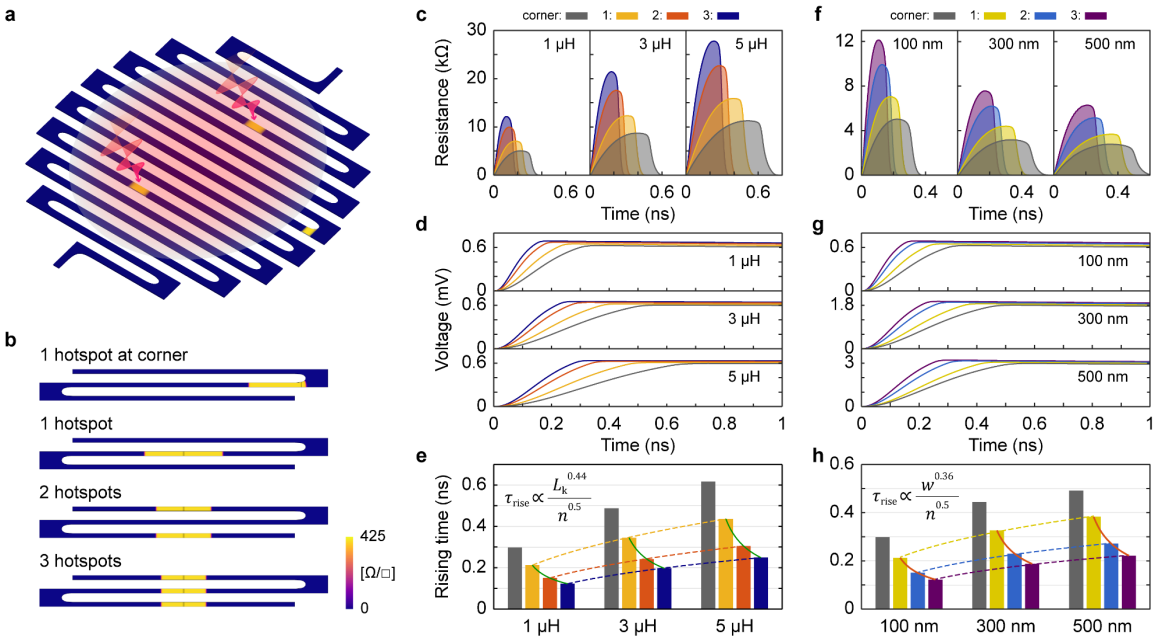

Fig. S3 | Electrothermal simulation results. a, Conceptual diagram of multi-photon detection. **b**, Simulated 2D profiles of sheet resistance when the total resistance reaches the maximum at different hotspot events. **c-e**, Simulated transient resistance (c), output electrical signals (d), and rising-edge time (e) of different hotspot events at different inductance. **f-h**, Simulated transient resistance (f), output electrical signals (g), and rising-edge time (h) of different hotspot events at different widths.